JACS
JOURNAL OF THE AMERICAN CHEMICAL SOCIETY
Article
Cite This: J. Am. Chem. Soc. 2017, 139, 18705−18713
pubs.acs.org/JACS

Privileged Role of Thiolate as the Axial Ligand in Hydrogen Atom Transfer Reactions by Oxoiron(IV) Complexes in Shaping the Potential Energy Surface and Inducing Significant H-Atom Tunneling

Johannes E. M. N. Klein,*[,†,§] Debasish Mandal,[‡,⊥] Wei-Min Ching,[†,∥] Dibyendu Mallick,[‡,#] Lawrence Que, Jr.,*[,†] and Sason Shaik*[,‡]

[†]Department of Chemistry and Center for Metals in Biocatalysis, University of Minnesota, Minneapolis, Minnesota 55455, United States

[‡]Institute of Chemistry and the Lise Meitner-Minerva Center for Computational Quantum Chemistry, The Hebrew University of Jerusalem, 91904 Jerusalem, Israel

Supporting Information

ABSTRACT: An H/D kinetic isotope effect (KIE) of 80 is found at −20 °C for the oxidation of 9,10-dihydroanthracene by $[Fe^{IV}(O)(TMCS)]^+$, a complex supported by the tetramethylcyclam (TMC) macrocycle with a tethered thiolate. This KIE value approaches that previously predicted by DFT calculations. Other $[Fe^{IV}(O)(TMC)(anion)]$ complexes exhibit values of 20, suggesting that the thiolate ligand of $[Fe^{IV}(O)(TMCS)]^+$ plays a unique role in facilitating tunneling. Calculations show that tunneling is most enhanced (a) when the bond asymmetry between C−H bond breaking and O−H bond formation in the transition state is minimized, and (b) when the electrostatic interactions in the O---H---C moiety are maximal. These two factors—which peak for the best electron donor, the thiolate ligand—afford a slim and narrow barrier through which the H-atom can tunnel most effectively.

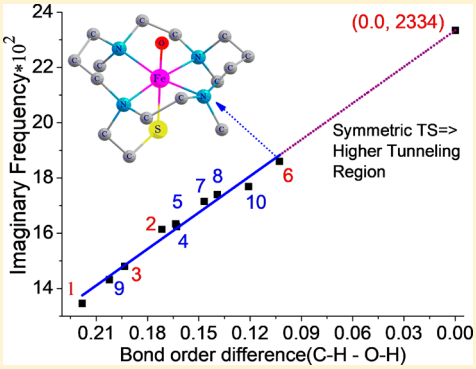

INTRODUCTION

Among the more challenging chemical transformations carried out by enzymes is the oxidative functionalization of inert C−H bonds,[1] including the hydroxylation of the very strong C−H bond (105 kcal mol^{-1}) in methane.[2,3] Due to the low mass of the hydrogen atom, tunneling, which is experimentally probed by measuring kinetic isotope effects (KIEs), can be a major contributor to faster reaction rates, selectivity, counterintuitive reactivity, etc.[4−9] Examples of enzymatic high-valent iron oxidants that exhibit KIEs with values as large as 100 in C−H bond oxidation reactions[10] include cytochromes P450 (CYPs, ∼15),[11] soluble methane monooxygenase (sMMO, ∼50),[12−14] taurine dioxygenase (TauD, ∼50),[15−17] and soybean lipoxygenase (SLO, ∼80).[18] For a double mutant of SLO, Hu et al. demonstrated KIEs approaching a value of 700.[19] Tunneling can therefore become a major factor in the ability of a given enzyme to perform challenging transformations of C−H bonds and can, if appropriately modulated by the environment, lead to enhanced selectivity for certain C−H bonds present in substrates that go beyond simple selectivity principles dominated by bond strength considerations.

Since the report of the X-ray structure[20] of the synthetic non-heme oxoiron(IV) complex $[Fe^{IV}(O)(TMC)(NCMe)]^{2+}$, **1-(NCMe)** in Figure 1a with an intermediate spin state (S = 1), related complexes bearing the TMC ligand framework have provided us with great insight into the C−H bond-cleaving reactivity of non-heme oxoiron(IV) complexes.[21,22] An early and puzzling observation was made in the investigation of the reactivities of a series of these complexes with varying axial ligands, L_{ax}, bound *trans* to the oxo ligand, namely L_{ax} = NCMe, N_3^-, $CF_3CO_2^-$, and thiolate.[23] For the last complex in the series, the thiolate moiety had to be tethered to the TMC framework in order to be observed.[24]

The studies of Sastri et al.[23] found that the second-order rate constant for oxygen atom transfer (OAT) to PPh_3 decreased as a more electron-donating axial ligand was employed, reflecting the diminishing electrophilicity of the Fe^{IV}=O unit. In stark contrast, an opposite trend was observed[23] for the oxidation of 9,10-dihydroanthracene (DHA), a hydrogen atom transfer (HAT) reaction, with the reaction rate increasing as the axial ligand became more electron-donating. As this trend was the opposite of that observed for the OAT rates, it was described as *anti-electrophilic* and was rationalized by invoking a change in spin state, from S = 1 to S = 2 en route to the transition state,[23] a phenomenon termed two-state reactivity (TSR)[25,26] and depicted schematically in Figure 2. More specifically it was argued early on that the spin state gap between the S = 1 and the S = 2 spin states (see $\Delta E_{(Q\text{-}T)}$ in Figure 2) would govern how reactive a given oxoiron(IV) complex of the TMC family would be toward C−H bonds.[23]

Received: October 23, 2017
Published: November 28, 2017

DOI: 10.1021/jacs.7b11300
J. Am. Chem. Soc. 2017, 139, 18705−18713

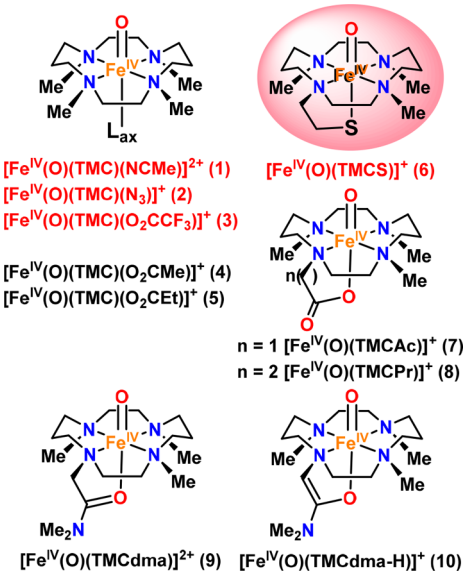

Figure 1. $[Fe(O)(TMC)(L_{ax})]^{Z+}$ (Z = 1. 2) complexes used in this study (with the bolded numbers in parentheses representing the oxidants in plots presented in later figures). Complexes marked in red refer to the original data reported by Sastri et al.[23]

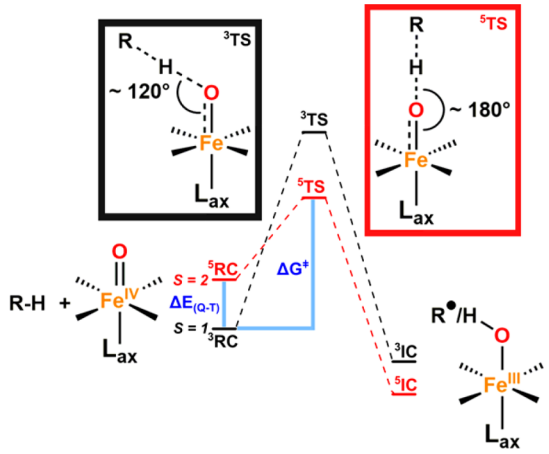

Figure 2. Generic TSR scenario for S = 1 non-heme oxoiron(IV) complexes. Adapted from ref 27.

Further support for this notion was achieved by increasing the number of experimentally studied TMC-based complexes from the original set of 4 to the current set of 10 (Figure 1) and comparing their observed reactivity properties with computational results.[28] These oxoiron(IV) complexes are depicted in Figure 1 and specified by their axial ligand, L_{ax}. A clear correlation between the spin-state splitting energy ($\Delta E_{(Q\text{-}T)}$) and the reactivity has been found previously, which supports the notion that the reaction occurs on the S = 2 spin surface.[28] However, this quantity is solely attributed to the isolated complex and can thus only be indirectly tied to the actual C−H bond breaking event in the transition state.

In an attempt to establish a more direct link between experiment and theory for the C−H bond cleavage, some of us had computed kinetic isotope effects (KIEs) for the oxidation of DHA by the aforementioned series of TMC-based complexes.[27] One major conclusion from that study is that the tunneling-augmented KIE value is a good probe of the reactive spin state, an approach that has more recently been applied to a variety of examples.[29−32] While the KIE values calculated for an S = 1 process of the $Fe^{IV}(O)(TMC)$ complexes shown in Figure 1 are 1−2 orders of magnitude larger than the experimental values obtained,[23] those calculated for a process starting on the S = 1 spin surface and going through the transition state on the S = 2 surface (^{5}TS) are in accord with known experimental values (Table 1). A particularly impressive example is the case of C−H bond oxidation of DHA by the oxoiron(IV) complex **3** bearing a trifluoroacetate axial ligand. A KIE of 1045 has been computed for the S = 1 spin state, compared to 16 computed for the S = 2 spin state,[28] and the latter is in excellent agreement with the experimental value of 19 reported by Sastri et al.[23]

Before proceeding, we note that this result does not necessarily mean that reactions proceeding on the S = 1 spin surface would always be expected to have such extreme KIEs for C−H bond oxidation. For other non-heme complexes, such as the oxoiron(IV) complex supported by the N4Py ligand (*N*,*N*-bis(2-pyridylmethyl)-*N*-bis(2-pyridyl)methylamine), the computed KIE for the S = 1 state actually matches the experimental data (55 ± 5) in the oxidation of the allylic C−H bond of cyclohexene, while the value calculated for the S = 2 state is much too small (~4).[31,33] Similarly, oxoiron(IV) porphyrin complexes have recently been predicted to exhibit a KIE = 33 for the S = 1 spin state at T = 288 K in DHA oxidation vs 4 for S = 2,[34] and the computed S = 1 value is comparable to the experimental one of 20.[35] From these data we can see that the potential energy surfaces (PESs) for the respective S = 2 spin states are shallower and less amenable to tunneling than the S = 1 spin states. Note however that, in contrast to most of the other synthetic non-heme oxoiron(IV)

Table 1. Comparison of Experimentally Determined and Computed KIEs for the C−H Bond Oxidation of DHA by Various TMC-Based Oxoiron(IV) Complexes

		KIE			ref	
complex	conditions	expt	calc	ν (imag), cm^{-1}	expt	.calc
$[Fe(O)(TMC)(NCMe)]^{2+}$	MeCN, 25 °C	10 (25 °C)	14.4 (25 °C)	1346	23	27
$[Fe(O)(TMC)(N_3)]^{+}$	MeCN, 0 °C	17 (0 °C)	22 (0 °C)	1614	23	27, 28
$[Fe(O)(TMC)(O_2CCF_3)]^{+}$	MeCN, 0 °C	19 (0 °C)	16 (0 °C)	1480	23	28
$[Fe(O)(TMC)(OAc)]^{+}$	MeCN, 0 °C	19 (0 °C)	30 (0 °C)	1634	28	28
$[Fe(O)(TMC)(OPr)]^{+}$	MeCN, 0 °C	17 (0 °C)	37 (0 °C)	1624	28	28
$[Fe(O)(TMCAc)]^{+}$	MeCN, 0 °C	~15 (0 °C)	38 (0 °C)	1715	28	28
$[Fe(O)(TMCPr)]^{+}$	MeCN, 0 °C	20 (0 °C)	39 (0 °C)	1740	28	28
$[Fe(O)(TMCS)]^{+}$	MeOH, −20 °C	80 (−20 °C)	98 (−20 °C)	1860	this work	27
	and 0 °C	~60 (0 °C)	61 (0 °C)			this work

DOI: 10.1021/jacs.7b11300
J. Am. Chem. Soc. 2017, 139, 18705−18713

cases, certain oxoiron(IV) systems with strongly donating macrocyclic ligands, both heme and non-heme, have $S = 2$ states that lie significantly higher in energy than the $S = 1$ spin state, resulting in single-state reactivity.[34,36−38] A notable feature of these complexes is the change in the ordering of the frontier molecular orbitals such that the $\sigma^*(d_{x^2-y^2})$ orbital is at higher energy than the $\sigma^*(d_{z^2})$ orbital. Thus, it is not a rule that $S = 2$ must be the reactive spin state of oxoiron(IV) complexes. As such, KIE determination by both experiment and theory constitutes a powerful tool to identify the reactive spin state.

Particular focus has been placed[27] on the connection between the KIE and the *anti-electrophilic* trend for C−H bond activation found for a series of $[Fe^{IV}(O)(TMC)(L_{ax})]$ complexes.[23] It was predicted that the KIE should increase with the electron-donating ability of the axial ligand (L_{ax} in Figure 1), more specifically in the order of KIE(MeCN) (**1**) < KIE(azide) (**2**) < KIE(thiolate) (**6**). The KIE for the reaction of the complex with L_{ax} = thiolate was calculated to be 51−61 (298 K) and significantly larger than those for the other ligands due to much more extensive tunneling in the case of the thiolate complex. Since tunneling "cuts through" the barrier (see Figure 3a), the effective barrier, $\Delta E^{\ddagger}_{eff}$, for the reaction of **6** becomes lower than the corresponding one for **1**. Furthermore, it is found that the tunneling effect on the barrier increases as the L_{ax} ligand becomes a better electron donor. Figure 3b shows the variation of the barrier cutting due to H-tunneling as a function of the donor-ability index of the axial ligand $\Delta q_{CT}(L_{ax})$. This index provides the calculated amount of charge transferred from the axial ligand to the rest of the iron-oxo complex upon coordination of L_{ax} to the oxoiron(IV) unit.[27] For thiolate a value of $\Delta q_{CT} = -1$ was calculated, whereas for NCMe only $\Delta q_{CT} = -0.3$ was obtained, which means that, upon coordination to the iron(IV) ion, thiolate transfers 1 e^- to the rest of the molecule, whereas NCMe transfers only 0.3 e^-. It has been argued that it is this L_{ax}-donicity-dependent tunneling effect on the barrier that is responsible for the observed *anti-electrophilic* effect, by rendering the effective H-abstraction barrier $\Delta E^{\ddagger}_{eff}$ lower for thiolate than for NCMe.

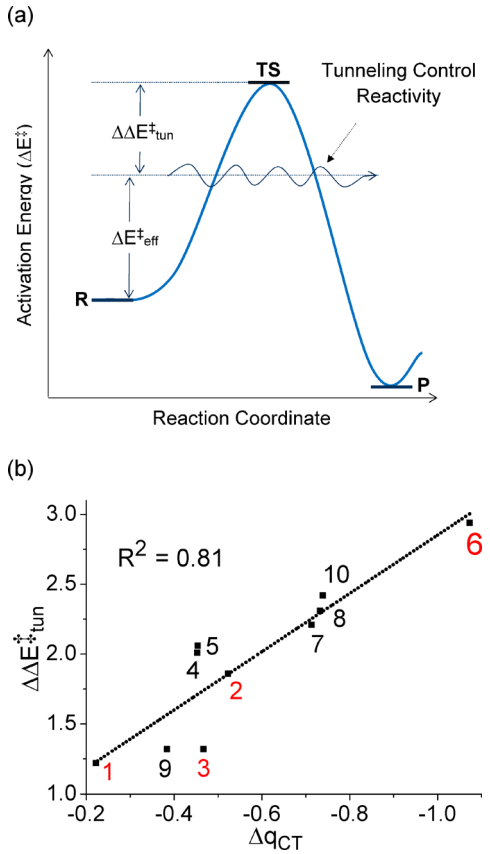

Figure 3. (a) Cartoon depicting barrier cutting due to H-tunneling. Reproduced with permission from ref 27 (Scheme 5). Copyright 2015 American Chemical Society. (b) The extent of barrier cutting due to tunneling, $\Delta\Delta E^{\ddagger}_{tun}$, vs the donor ability $\Delta q_{CT}(L_{ax})$ of the axial ligand (calculated using NBO at the UB3LYP/LACVP* level of theory) on the $[Fe(O)(TMC)(L_{ax})]^{Z+}$ complexes (Z = 1, 2).

At that point in time, experimental KIE values were available only for complexes bearing axial MeCN, azide and trifluoroacetate ligands. As mentioned already, these values matched the computed ones only for the $S = 2$ spin surface, as the computed values for the $S = 1$ spin surface were much, much higher.[27] In our recent study, where the number of complexes in the TMC series was increased to 10,[28] we reported experimental and computed KIEs for DHA oxidation for a series of carboxylate-substituted complexes. One of the noteworthy comparisons was between complexes with axial ligands that were either free or covalently attached to the TMC framework. For example, in the case of the acetate ligand, we observed a 100-fold rate difference between the tethered and untethered cases.[28] Despite this significant difference in reactivity, both complexes exhibited very similar KIEs, suggesting that the difference in reactivity is caused by the geometrical constraint imposed by tethering the axial ligand and not by the nature of the axial ligand itself. While we were able to establish that there are factors influencing reactivity that go beyond simply the type of axial ligand, we also showed that tunneling can contribute to reactivity by lowering the activation barrier, approximately to the same extent, 2−2.9 kcal mol^{-1}, for all the carboxylate-type ligands.[28] We recall that, for complex **6** with axial thiolate, the best donor ligand in the series in Figure 1, the barrier was predicted to be lowered by 3.4−3.5 kcal mol^{-1} relative to the parent complex featuring a MeCN ligand in the axial position, the largest difference in the series.[27]

In the present Article we report the KIE for DHA oxidation by **6** to obtain experimental evidence for the theoretical prediction.[27] We also derive a physical basis for how the axial ligands can alter the tunneling contribution and KIE and ultimately give rise to rate enhancements by inducing nonclassical and counterintuitive behavior. Our findings have direct implications for thiolate-ligated high-valent iron centers in biological systems and provide a basis for experimentally observed trends.

RESULTS

In our efforts to further understand how the axial ligand affects the reactivity of the oxoiron(IV) unit and, more specifically, how it modulates the KIE in C−H bond activation, we began by first establishing an experimental basis by determining the KIE for the $[Fe(O)(TMCS)]^+$ complex (**6**) where TMCS is TMC with an appended L_{ax} = thiolate (for a structure see Figure 1). The experimental and computational details are given in the Methods section.

We judge this $[Fe(O)(TMCS)]^+$ complex[24] to be of particular relevance to this effort, as it is predicted to exhibit a theoretical KIE that is substantially higher than for complexes

DOI: 10.1021/jacs.7b11300
J. Am. Chem. Soc. 2017, 139, 18705−18713

with other axial ligands.[27] It is also noteworthy that this complex represents the only well characterized example to date of a high-valent non-heme oxoiron(IV) complex with an axial thiolate ligand, reminiscent of the iron coordination environment in a variety of heme-based biological systems.[39−41] Early work by Woggon and co-workers focused on synthetic models of P450s and chloroperoxidase (CPO) featuring axially bound thiolate ligands.[42] In their studies, it was indeed possible to observe the formation of an intermediate with an absorption at λ_{max} at 388 nm,[43] which compares well to the feature attributed to Compounds I in cytochrome P450[44] and CPO[45] with a value of 367 nm. However, no C−H bond reactivity studies were reported.

Our endeavor turned out to be particularly challenging due to the significantly more fragile nature of complex **6**. The originally reported reaction conditions for the oxidation of DHA by Sastri et al. used a 1:1 mixture of MeCN and MeOH at 0 °C.[23] Under these conditions, the reaction of **6** with DHA was not sufficiently well behaved in our hands, and a reliable KIE value could not be obtained. We thus switched to pure MeOH as the solvent and explored reaction temperatures of 0 °C and −20 °C. Under these conditions, we were indeed able to determine the KIE for the oxidation for DHA to be 80 at −20 °C (Figure 4) and estimate a KIE of ∼60 for the reaction

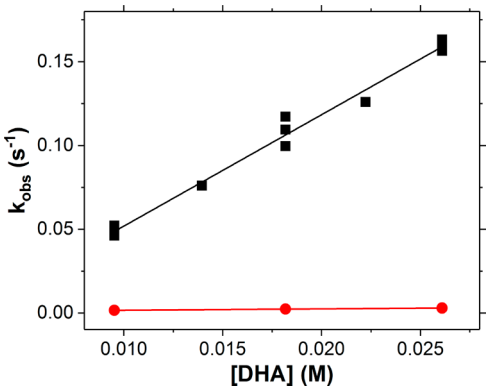

Figure 4. Representative k_2 plots for the reactions of [Fe(O)(TMCS)]$^+$ in CD_3OH with varying amounts of DHA-h_4 (black squares) and DHA-d_4 (red dots) at −20 °C.

at 0 °C. We note that the rates at 0 °C became relatively fast compared to the mixing times following addition of DHA solutions only allowing us to estimate a KIE (see Figure S1). A KIE value of 80 at −20 °C is a factor of 4 higher than found for the other complexes with anionic axial ligands and a factor of 8 larger than that for the parent MeCN complex. These results match the theoretically computed KIE_{th} values.

The KIE value obtained at −20 °C (KIE_{exp} = 80) is comparable to the value of 60 computed for 25 °C by Mandal et al. in their first report.[27] This result shows that the originally observed *anti-electrophilic* trend is due to a barrier slicing effect by tunneling, which depends on the nature of the axial ligand. Having established this experimental basis, we recomputed the KIE for the [Fe(O)(TMCS)]$^+$ complex at −20 °C and obtained a value of 98, in reasonable agreement with experiment (Table 1). In addition, we also reevaluated the calculated KIE at 0 °C, for which we obtained a value of 61 comparing well to our experimental estimation of ∼60. These data thus suggest that we do capture the temperature dependence of the KIEs reasonably well and provide further validation for the computational approach chosen.

Having validated the previous prediction, we are now in a position to ask the question: How does the nature of the axial ligand cause a large KIE in C−H bond oxidation reactions? And maybe more importantly: What are the implications for reactivity and selectivity? For this purpose we might group the complexes that have been studied into three subsets: (i) The parent complex [Fe(O)(TMC)(NCMe)]$^{2+}$ with a moderate KIE of 10 (25 °C), (ii) complexes with azide or carboxylate-derived axial ligands, which range from ∼15 to 20 (0 °C), and (iii) the [Fe(O)(TMCS)]$^+$ complex, which has a KIE of 80 (−20 °C). All computed KIEs are for the S = 2 spin state, which we have clearly identified as the reactive spin state as outlined in the introduction.

Figure 5 shows the connection between the donor property of the axial ligand and the quantities that determine tunneling

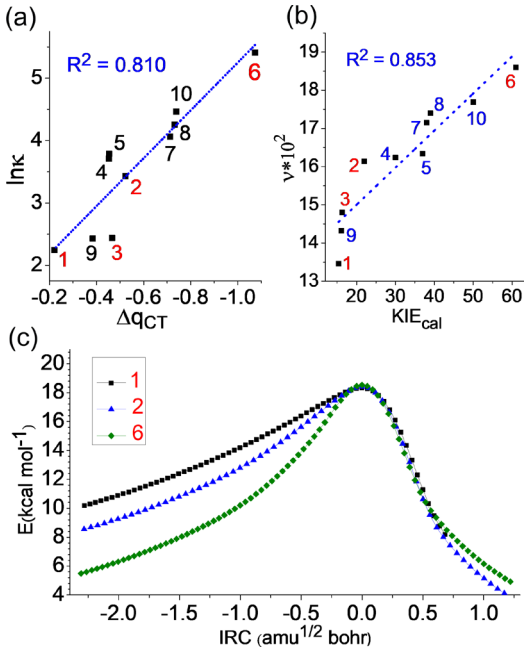

Figure 5. (a) Plot of the logarithm of the H-transmission coefficient for tunneling vs Δq_{CT}. (b) Plot of the absolute magnitude of the imaginary frequency (in cm^{-1}) vs KIE_{cal} at T = 273 K. (c) Plots of the barriers vs the intrinsic reaction coordinate (IRC) for the reactions of DHA with three Fe^{IV}(O)TMC complexes in the series. Here, the upper points of the plots are normalized to show more clearly the effect of the axial ligand on the barrier width. This plot is adapted from Figure S8 in ref 27. with permission from the American Chemical Society.

efficiency and KIE, using three frames taken from our previous study.[27] Figure 5a shows that the transmission coefficient κ (for tunneling) increases steeply with $\Delta q_{CT}(L_{ax})$, and the highest κ is obtained for [Fe(O)(TMCS)]$^+$, which possesses an axial thiolate ligand, the most electron-donating axial ligand in the series. Figure 5b displays a plot of the imaginary frequency vs the calculated KIE values at 273 K presented in the Supporting Information (SI). It is apparent that the calculated tunneling is dominated by the imaginary frequency in the corresponding ^5TS_H. Thus, the TS for the complex with the best donor L_{ax}, [Fe(O)(TMCS)]$^+$, possesses the highest imaginary frequency in the set and the highest KIE at a given temperature. Nevertheless, there is some scatter in the plot near the lower

DOI: 10.1021/jacs.7b11300
J. Am. Chem. Soc. 2017, 139, 18705−18713

end of the KIE, which indicates that there are secondary effects that modulate the tunneling for a given imaginary frequency. Figure 5c reveals such a factor by showing the potential energy curves of a few of the H-abstraction reactions plotted along the intrinsic reaction coordinate (IRC). It is seen that the barrier for $[Fe(O)(TMCS)]^+$ stands out, as it is the least asymmetric and quite narrow virtually throughout its height. On the other hand, all other ligands lead to a more asymmetric barrier that diverges close to its top and becomes broad. The most asymmetric and broadest barrier is for $[Fe(O)(TMC)(NCMe)]^{2+}$, which possesses the weakest electron donor axial ligand. As such, the $[Fe(O)(TMCS)]^+$ barrier is ideal for tunneling, while the other oxoiron(IV) complexes have decreased tunneling efficiency.

Using all the above trends, we now attempt to formulate a more chemically intuitive model for the behavior displayed in Figure 5. Thus, if we simply reflect the barrier through a mirror passing perpendicular to the plane of the page, the barrier will "become" a minimum. As such, the imaginary frequency, which determines the curvature of the barrier near the TS, can be regarded as though it were a real frequency of a stable structure located at an energy minimum. Therefore, we shall try to link the foregoing features of the barrier to physical properties of the ^5TS_H.

As shown above (Figure 3), the properties of the TS are determined by the ability of the axial ligand, L_{ax}, to donate charge to the rest of the oxoiron(IV) complex. Indeed, the O---H---C moiety carries partial negative charges on O and C and a partial positive charge on H. In addition, the bond orders of the H in transit to O and C may be affected by the axial ligand and give rise to bond asymmetry of the TS. Let us therefore focus on the impact of the electrostatic energy in the TS on the corresponding imaginary frequency and then proceed to the TS bond order effects.

As expressed by eq 1a, the electrostatic potential energy V varies in proportion to the products of the charges on O, H, and C, with a distance dependence of $1/R$, where the R's are the corresponding distances across the $O^{Q-}\cdots H^{Q+}\cdots C^{Q-}$ moiety.

$$V = -\frac{|Q_O| \times |Q_H|}{R_{O-H}} - \frac{|Q_C| \times |Q_H|}{R_{C-H}} + \frac{|Q_C| \times |Q_O|}{R_{C-O}} \quad (1a)$$

Assuming other interactions are constant, the second derivative of V will dominate the force constant (k) of the $O^{Q-}\cdots H^{Q+}\cdots C^{Q-}$ moiety and will be proportional to the sum of the first two charge products (see SI for details), which are responsible for electrostatic stabilization (eq 1b):

$$\frac{d^2V}{dR^2} \approx k \propto -[|Q_O Q_H| + [|Q_C Q_H|] \quad (1b)$$

Figure 6 summarizes our insight into the factors that slim the barrier. Figure 6a shows a reasonable correlation of the squared imaginary frequencies with the sum of the product charge in eq 1b, while Figure 6b shows the correlation with the full second derivative of the electrostatic potential (for a detailed derivation see SI). The good correlation implies electrostatic narrowing of the barrier. Thus, as the axial ligand's donicity increases, the electrostatic interaction across O---H---C becomes more stabilizing and the corresponding imaginary frequency becomes larger, and vice versa. It is seen that the TS for $[Fe(O)(TMCS)]^+$ has the most negative electrostatic potential, and

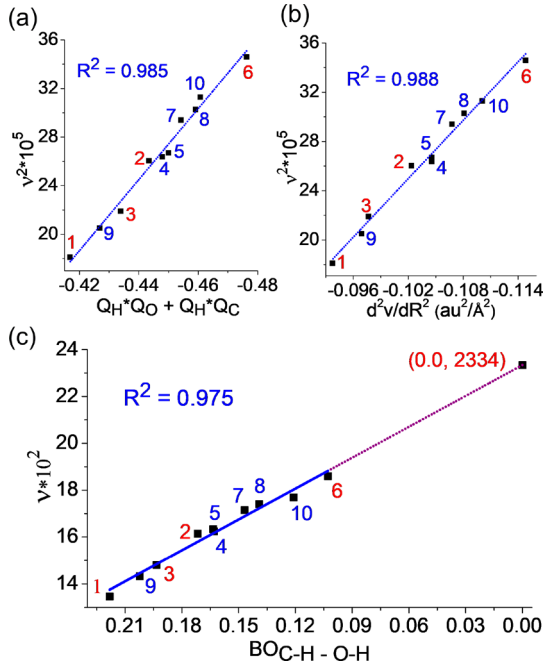

Figure 6. (a) Correlation of the square of the imaginary frequency (in cm^{-1}) with the electrostatic potential (V) across the O---H---C moiety in the TS, charge product $Q_HQ_O + Q_HQ_C$. (b) Correlation of the square of the imaginary frequency with the second derivative of V. (c) Correlation of the imaginary frequency with the difference of the C---H and H---O bond orders (BOs) in ^5TS_H. Extrapolation to zero asymmetry shows that such a putative TS will possess an imaginary frequency of 2334 cm^{-1}.

hence the highest imaginary frequency and the narrowest barrier, which are most conducive for efficient tunneling.

Figure 6c shows a plot of the imaginary frequency vs the difference between the C---H and H---O bond orders in the TS. The larger the bond order difference, the greater the asymmetry of the corresponding barrier (compare with Figure 5c),[9,46] which may also be associated with TSs that become late or early. The asymmetric barriers are broader than the symmetric barriers, and their corresponding imaginary frequencies are generally lower. Clearly, the bonding asymmetry in the TS acts as a factor that broadens the barrier and limits the energy space through which tunneling may occur. In this respect, it is seen that once again the TS of $[Fe(O)(TMCS)]^+$ stands out as the one having the least asymmetry. As a result, the corresponding barrier is the narrowest and the most symmetric one in the set. An ideal scenario in this series would be one with a fully symmetric TS and an imaginary frequency extrapolated to 2334 cm^{-1}, leading to facile tunneling and a large KIE.

Our observations also provide us with a perspective on the role of the axial ligand for the thiolate-ligated active sites of cytochrome P450 versus histidine-ligated centers in heme peroxidases. In line with the reactivity trends observed in the series of TMC-based complexes presented in this study, the heme-based systems also exhibit increased C−H bond activation reactivity in the presence of the strongly donating thiolate ligand.[40,41] To date no reactivity data are available for synthetic models of the high-valent intermediate, Compound I, with an axial thiolate ligand, making the experimental exploration of the axial ligand effect for this strongly donating variant challenging (*vide supra*). On the other hand, a more electron-donating selenolate axial ligand has recently been

DOI: 10.1021/jacs.7b11300
J. Am. Chem. Soc. 2017, 139, 18705−18713

introduced into cytochrome P450.[47−54] Green and co-workers have provided spectroscopic evidence for the formation of the corresponding Compound I species and found an increased reactivity toward C−H bonds.[55] Based on the above discussion, we expect that increasing the donicity of the axial ligand from cysteine to selenocysteine will enhance the tunneling efficiency. Indeed, in synthetic Compound I complexes, it is observed that making the ligands to the high-valent Fe center more electron-donating, by introducing either appropriate axial ligands or meso substituents on the porphyrin, increased tunneling in H-abstraction reactions.[56,57] It is expected therefore that the selenocysteine-Compound I will have a higher tunneling contribution to H-abstraction reactivity.

The same notions also apply to isopenicillin N synthase (IPNS),[58−62] another C−H bond-cleaving iron enzyme that generates an oxoiron(IV) oxidant.[63] In this case, a substrate-derived thiolate is coordinated *cis* to the incipient oxo atom[59,61] and gives rise to a KIE for C−H bond oxidation by this high-valent intermediate that is estimated to be >30.[63] Thus, IPNS represents another instance of a biological iron oxidant with a thiolate ligand that gives rise to a significant tunneling component in the transition state.

Even without employing a thiolate ligand, biology has been able to tune a metalloenzyme active site to elicit significant tunneling contributions in the cleavage of a substrate C−H bond. Examples include soybean lipoxygenase at one extreme, which cleaves the weak allylic C−H bonds of linoleic acid (BDE ≈ 80 kcal mol^{-1}) with a KIE of 80,[18] and sMMO at the other extreme, which carries out the most challenging transformation of breaking the very strong C−H bond of methane (BDE = 105 kcal mol^{-1}) with a KIE of 50.[12−14] As we have demonstrated, greater tunneling contributions arise from a more symmetrical transition state. Therefore, for an active site that has evolved to break a specific C−H bond in a substrate, matching the oxidant's nature to this specific C−H bond can contribute substantially to the high levels of selectivity achieved by enzymes.

Thus, it is remarkable that the high-valent diiron oxidant **Q** of sMMO may attack the very strong C−H bond of methane specifically without oxidizing the weaker C−H bonds within the active site. It has been proposed that the actual active oxidant is unmasked only after methane enters the active site in order to minimize collateral damage.[14,64−66] In light of the presented results, one might add to the previous proposal that in high-valent iron active sites engaged in C−H bond activation, matching the nature of the oxidant to its specific substrate can result in enhanced specificity due to tunneling contributions.

The principles described are not to be mistaken for a peculiarity in biological systems,[67] but also provide a general platform for approaching high levels of selectivity for nonbiological reactions involving C−H bond activation. This notion is corroborated for the synthetic oxoiron(IV) complex [Fe^{IV}(O)(BnTPEN)]$^{2+}$ by the experimental observation that an inverted V-shaped plot of the KIE values vs the C−H bond strengths of a variety of substrates has been observed experimentally[68] and corroborated computationally.[31] Although controversial, the term "quantum catalysis" has previously been associated with such phenomena.[8,69,70]

In summary, therefore, Figure 6 shows that electrostatic interactions contribute to sculpting of the narrowness of the barrier near the TS, affecting the imaginary frequency and hence the shape of the PES. On the other hand, the bonding asymmetry in the TS causes the barrier to extend in a given direction of the IRC and minimize the narrow part of the barrier that is available for tunneling. Thus, as the axial ligand of [Fe(O)(TMC)(L$_{ax}$)]$^{z+}$ becomes a better electron donor, it increases the electrostatic interaction that leads to a narrow barrier and reduces the binding asymmetry of the H in transit, thereby leading to a higher tunneling efficiency and KIE. In this study of various complexes that abstract an H-atom from DHA, [Fe(O)(TMCS)]$^{+}$ (**6**) is the most ideal complex for tunneling controlled-reactivity.

■ CONCLUSIONS

We have presented here experimental verification of an earlier DFT prediction that the KIE value for the reactions of [Fe(O)(TMCS)]$^{+}$ with hydrocarbons is the highest among all the known [Fe(O)(TMC)(L$_{ax}$)]$^{z+}$ complexes.[27] Having done that, we have presented an intuitive model of the factors that control tunneling in these systems. One factor is the electrostatic stabilization of the H$^{\delta+}$ as it moves between the C$^{\delta-}$ and O$^{\delta-}$ moieties in the TS. The greater the electrostatic stabilization, the narrower the barrier and the larger the imaginary frequency it would possess, leading to larger tunneling. The second factor is the symmetry of the energy barrier, which as we showed is controlled by the bond order (BO) differences of the two bonds to H in the TS, namely, BO(C---H) − BO(H---O). The smaller the difference, the more symmetric is the TS and the larger would be the tunneling contribution. As we demonstrate, when the axial ligand of the oxoiron(IV) complex is a good electron donor, both of the aforementioned factors favor tunneling. Indeed, the highest tunneling is *observed and computed* for [Fe(O)(TMCS)]$^{+}$ in its reaction with DHA. This dependence of the tunneling on the donicity of the axial ligand is responsible for the anti-electrophilic reactivity trend, noted previously for the H-abstraction reactions of [Fe(O)(TMC(L$_{ax}$)]$^{Z+}$.[23] Clearly, tunneling operates here as a selectivity parameter, as shown by Schreiner et al.[8]

■ METHODS

Experimental Details. Reagents and solvents were obtained from commercial suppliers and used as received unless specified. 9,10-Dihydroanthracene (DHA) was purified by recrystallization from hot EtOH under an argon atmosphere, and residual EtOH was removed via co-evaporation with benzene. DHA-d_4 was prepared as described in the literature,[66] and purified as its hydrogen isotopologue. *meta*-Chloroperoxybenzoic acid (*m*-CPBA) was purified prior to use as outlined in ref 71. The purity of the *m*-CPBA was assessed by reacting it with PPh_3 and determining the amount of $OPPh_3$ formed. [Fe^{II}(TMCS)]PF_6 was prepared following reported procedures.[72,73] Second-order rate constants for the oxidation of DHA and DHA-d_4 were obtained by monitoring UV−vis absorption spectra on a HP 8453A diode array spectrometer equipped with a cryostat from UNISOKU Scientific Instruments, Japan. In a representative kinetic run, a UV−vis cuvette was charged with 1 mL of a 1 mM stock solution inside an N_2-filled glovebox and sealed with a septum. The cuvette was placed inside the spectrometer and cooled to −20 °C (or 0 °C). Then KO*t*Bu (6 equiv) and *m*-CPBA (1 equiv) were added as stock solutions in MeOH. The formation of the [Fe^{IV}(O)(TMCS)]$^{+}$ species[24,74] was monitored, and upon maximum formation DHA-(h_4 or d_4) was added as a stock solution in benzene. Note that benzene was used to ensure solubility of DHA in MeOH under the reaction conditions. Stock solutions of KO*t*Bu and *m*-CPBA were cooled to ∼0 °C and stock solutions of DHA-(h_4 or d_4) were maintained just above the melting point of benzene. Decay profiles were fit to a single exponential for approximately five half-lives after mixing. Representa-

DOI: 10.1021/jacs.7b11300
J. Am. Chem. Soc. 2017, 139, 18705−18713

tive plots of k_{obs} vs [DHA] for the determination of second-order rate constants can be found in the SI.

Computational Details. Previously, several data for TMC complexes were reported by us for different substrates, calculated at different levels of theory and more specifically for different purposes.[27,28,31] Here we have performed complete investigations at a uniform level of theory for all the TMC systems and using a common substrate DHA for all types of calculations. All calculations, except for the optimizations of the stationary states and NBO for a few oxidants, are new, and the reported data may not be exactly identical with those reported in our previous investigations. The following details are to follow this Article independently.

General Notes on Calculations. Geometry optimizations were carried out with the Jaguar 8.0 program[75,76] package with the UB3LYP[77−79] density functional and the LACVP*(Fe)/6-31G*(rest) basis set.[80−82] We neutralized here the charge of the iron(IV)-oxo reagents with $CF_3SO_3^-$ counterions in order to reduce self-interaction error[83−85] and verified that there are no further consequences on reactivity. A subsequent frequency calculation was also done at the same level to confirm the nature of the optimized structures as local minima (no imaginary frequency) or transition states (one imaginary frequency), and to evaluate the zero point vibrational energy (ZPVE), as well as thermal and entropic corrections to the Gibbs free energy. Intrinsic reaction coordinates (IRCs) were calculated using HPC algorithm[86−88] and mass-weighted Cartesian coordinates, which is the default choice in Gaussian 09.[89] More than 200 steps were calculated with step sizes of 5 (0.005 $amu^{1/2}$ Bohr) to check that the transition states exactly correlate with the reactants and intermediates.

Tunneling Corrections and Kinetic Isotope Effect (KIE) Calculations. Eckart tunneling calculations were performed using TheRate program.[90] The Eckart-based method[91] uses an analytical potential energy function fitted by the computed and ZPVE corrected energies of the reactant, products, and TS, as well as by the imaginary frequency along the adiabatic minimum energy pathway, i.e., the intrinsic reaction coordinate (IRC), in mass-weighted Cartesian coordinates. Using the definitions in this paper, the Eckart function is fitted at the E level. The transmission coefficient, κ, due to tunneling is calculated by integration of the barrier "penetration" probability as a Boltzmann-averaged function of the energy. The effect of the transmission coefficient κ on the barrier is calculated by the following equation:

$$\Delta\Delta E^{\ddagger}_{tun} = -RT \ln \kappa(T) \quad (2)$$

Here, R is the universal gas constant and T the absolute temperature. As can be seen from eq 2, the tunnelling correction effectively cuts the barrier by the quantity $\Delta\Delta E^{\ddagger}_{tun}$. Information regarding the reliability of the Eckart method relevant to these types of systems is given in the SI.

Corresponding kinetic isotopic effects (KIEs) were calculated for all the reactions and compared with available experimental data to ascertain the reliability of the tunneling contribution. The KIE calculations employed the frequencies of the reactions of the iron(IV)-oxo complexes with DHA and their deuterated isotopologue DHA-d_4. The KIEs were calculated using the semiclassical Eyring equation,[92] followed by tunneling-corrected (TC) values, using the following expression:

$$KIE_{TC} = (\kappa_H/\kappa_D)KIE_{EY} \quad (3)$$

where κ_H and κ_D are the transmission coefficients of the two isotopomers, evaluated by the Eckart method. The KIEs were calculated according to the available experimental temperature.

Atomic charges were calculated with NBO 3.1.[93] Bond order refers to Wiberg's bond orders.[94] Both were calculated at the aforementioned level of theory using GAUSSIAN 09.[89]

■ ASSOCIATED CONTENT

Supporting Information

The Supporting Information is available free of charge on the ACS Publications website at DOI: 10.1021/jacs.7b11300.

A detailed validation of the Eckart model as a tool for the determination of KIEs for C−H bond oxidation by oxoiron(IV) complexes, additional details on calculations, and Cartesian coordinates (PDF)

■ AUTHOR INFORMATION

Corresponding Authors

*j.e.m.n.klein@rug.nl
*larryque@umn.edu
*sason@yfaat.ch.huji.ac.il

ORCID

Johannes E. M. N. Klein: 0000-0002-1290-597X
Wei-Min Ching: 0000-0002-5299-4479
Dibyendu Mallick: 0000-0002-0650-1872
Lawrence Que Jr.: 0000-0002-0989-2813
Sason Shaik: 0000-0001-7643-9421

Present Addresses

§J. E. M. N. Klein: Molecular Inorganic Chemistry, Stratingh Institute for Chemistry, Faculty of Science and Engineering, University of Groningen, Nijenborgh 4, 9747 AG Groningen, The Netherlands
⊥D. Mandal: Computational Toxicology Facility, Indian Institute of Toxicology Research, Lucknow 226 001, India
∥W.-M. Ching: Instrumentation Center, Department of Chemistry, National Taiwan Normal University, Taipei 11677, Taiwan
#D. Mallick: School of Chemistry and Biochemistry, Thapar Institute of Engineering and Technology, Patiala 147 004, Punjab, India

Notes

The authors declare no competing financial interest.

■ ACKNOWLEDGMENTS

This work was supported at the University of Minnesota by grants from the U.S. National Science Foundation (CHE-1361773 and 1665391 to L.Q.), a Feodor Lynen Research Fellowship from the Alexander von Humboldt Foundation to J.E.M.N.K., and a postdoctoral fellowship to W.-M.C. from the Ministry of Science and Technology, Taiwan. S.S. acknowledges support from the Israel Science Foundation (ISF grant 1183/13).

■ REFERENCES

(1) Lewis, J. C.; Coelho, P. S.; Arnold, F. H. *Chem. Soc. Rev.* **2011**, *40*, 2003.
(2) Luo, Y.-R. *Comprehensive Handbook of Chemical Bond Energies*; CRC Press, Taylor & Francis Group: Boca Raton, FL, 2007.
(3) Wang, V. C. C.; Maji, S.; Chen, P. P. Y.; Lee, H. K.; Yu, S. S. F.; Chan, S. I. *Chem. Rev.* **2017**, *117*, 8574.
(4) O'Ferrall, R. A. M. *J. Phys. Org. Chem.* **2010**, *23*, 559.
(5) Simmons, E. M.; Hartwig, J. F. *Angew. Chem., Int. Ed.* **2012**, *51*, 3066.
(6) Meisner, J.; Kästner, J. *Angew. Chem., Int. Ed.* **2016**, *55*, 5400.
(7) McMahon, R. J. *Science* **2003**, *299*, 833.
(8) Ley, D.; Gerbig, D.; Schreiner, P. R. *Org. Biomol. Chem.* **2012**, *10*, 3781.
(9) Kozuch, S. *Phys. Chem. Chem. Phys.* **2014**, *16*, 7718.
(10) Lyakin, O. Y.; Shteinman, A. A. *Kinet. Catal.* **2012**, *53*, 694.
(11) Guengerich, F. P. *J. Labelled Compd. Radiopharm.* **2013**, *56*, 428.
(12) Nesheim, J. C.; Lipscomb, J. D. *Biochemistry* **1996**, *35*, 10240.
(13) Brazeau, B. J.; Lipscomb, J. D. *Biochemistry* **2003**, *42*, 5618.
(14) Zheng, H.; Lipscomb, J. D. *Biochemistry* **2006**, *45*, 1685.

DOI: 10.1021/jacs.7b11300
J. Am. Chem. Soc. 2017, 139, 18705−18713

(15) Price, J. C.; Barr, E. W.; Glass, T. E.; Krebs, C.; Bollinger, J. M., Jr. *J. Am. Chem. Soc.* **2003**, *125*, 13008.
(16) Bollinger, J. M.; Krebs, C. *J. Inorg. Biochem.* **2006**, *100*, 586.
(17) Krebs, C.; Galonić Fujimori, D.; Walsh, C. T.; Bollinger, J. M., Jr. *Acc. Chem. Res.* **2007**, *40*, 484.
(18) Knapp, M. J.; Rickert, K.; Klinman, J. P. *J. Am. Chem. Soc.* **2002**, *124*, 3865.
(19) Hu, S.; Soudackov, A. V.; Hammes-Schiffer, S.; Klinman, J. P. *ACS Catal.* **2017**, *7*, 3569.
(20) Rohde, J.-U.; In, J.-H.; Lim, M. H.; Brennessel, W. W.; Bukowski, M. R.; Stubna, A.; Münck, E.; Nam, W.; Que, L., Jr. *Science* **2003**, *299*, 1037.
(21) McDonald, A. R.; Que, L., Jr. *Coord. Chem. Rev.* **2013**, *257*, 414.
(22) Klein, J. E. M. N.; Que, L., Jr. Biomimetic High-Valent Mononuclear Nonheme Iron-Oxo Chemistry. *Encyclopedia of Inorganic and Bioinorganic Chemistry*; John Wiley & Sons, Ltd.: Chichester, UK, 2016; DOI: 10.1002/9781119951438.eibc2344.
(23) Sastri, C. V.; Lee, J.; Oh, K.; Lee, Y. J.; Lee, J.; Jackson, T. A.; Ray, K.; Hirao, H.; Shin, W.; Halfen, J. A.; Kim, J.; Que, L., Jr.; Shaik, S.; Nam, W. *Proc. Natl. Acad. Sci. U. S. A.* **2007**, *104*, 19181.
(24) Bukowski, M. R.; Koehntop, K. D.; Stubna, A.; Bominaar, E. L.; Halfen, J. A.; Münck, E.; Nam, W.; Que, L., Jr. *Science* **2005**, *310*, 1000.
(25) Schröder, D.; Shaik, S.; Schwarz, H. *Acc. Chem. Res.* **2000**, *33*, 139.
(26) Shaik, S. *Int. J. Mass Spectrom.* **2013**, *354*−*355*, 5.
(27) Mandal, D.; Ramanan, R.; Usharani, D.; Janardanan, D.; Wang, B.; Shaik, S. *J. Am. Chem. Soc.* **2015**, *137*, 722.
(28) Bigelow, J. O.; England, J.; Klein, J. E. M. N.; Farquhar, E. R.; Frisch, J. R.; Martinho, M.; Mandal, D.; Münck, E.; Shaik, S.; Que, L. *Inorg. Chem.* **2017**, *56*, 3287.
(29) Shaik, S.; Hirao, H.; Kumar, D. *Acc. Chem. Res.* **2007**, *40*, 532.
(30) Usharani, D.; Wang, B.; Sharon, D. A.; Shaik, S. *Spin States in Biochemistry and Inorganic Chemistry*; John Wiley & Sons, Ltd.: Chichester, UK, 2015; p 131.
(31) Mandal, D.; Shaik, S. *J. Am. Chem. Soc.* **2016**, *138*, 2094.
(32) Kim, Y.; Mai, B. K.; Park, S. *JBIC, J. Biol. Inorg. Chem.* **2017**, *22*, 321.
(33) Kwon, Y. H.; Mai, B. K.; Lee, Y.-M.; Dhuri, S. N.; Mandal, D.; Cho, K.-B.; Kim, Y.; Shaik, S.; Nam, W. *J. Phys. Chem. Lett.* **2015**, *6*, 1472.
(34) Mallick, D.; Shaik, S. *J. Am. Chem. Soc.* **2017**, *139*, 11451.
(35) Jeong, Y. J.; Kang, Y.; Han, A.-R.; Lee, Y.-M.; Kotani, H.; Fukuzumi, S.; Nam, W. *Angew. Chem., Int. Ed.* **2008**, *47*, 7321.
(36) Kupper, C.; Mondal, B.; Serrano-Plana, J.; Klawitter, I.; Neese, F.; Costas, M.; Ye, S.; Meyer, F. *J. Am. Chem. Soc.* **2017**, *139*, 8939.
(37) Ye, S.; Kupper, C.; Meyer, S.; Andris, E.; Navrátil, R.; Krahe, O.; Mondal, B.; Atanasov, M.; Bill, E.; Roithová, J.; Meyer, F.; Neese, F. *J. Am. Chem. Soc.* **2016**, *138*, 14312.
(38) Chanda, A.; Shan, X.; Chakrabarti, M.; Ellis, W. C.; Popescu, D. L.; de Oliveira, F. T.; Wang, D.; Que, L., Jr.; Collins, T. J.; Münck, E.; Bominaar, E. L. *Inorg. Chem.* **2008**, *47*, 3669.
(39) *Cytochrome P450: Structure, Mechanism, and Biochemistry*, 3rd ed.; Ortiz de Montellano, P. R., Ed.; Kluwer Academic/Plenum Publishers: New York, 2005.
(40) Groves, J. T. *Nat. Chem.* **2014**, *6*, 89.
(41) Yosca, T. H.; Ledray, A. P.; Ngo, J.; Green, M. T. *JBIC, J. Biol. Inorg. Chem.* **2017**, *22*, 209.
(42) Woggon, W.-D.; Wagenknecht, H.-A.; Claude, C. *J. Inorg. Biochem.* **2001**, *83*, 289.
(43) Wagenknecht, H.-A.; Woggon, W.-D. *Angew. Chem., Int. Ed. Engl.* **1997**, *36*, 390.
(44) Rittle, J.; Younker, J. M.; Green, M. T. *Inorg. Chem.* **2010**, *49*, 3610.
(45) Palcic, M. M.; Rutter, R.; Araiso, T.; Hager, L. P.; Dunford, H. B. *Biochem. Biophys. Res. Commun.* **1980**, *94*, 1123.
(46) Álvarez-Barcia, S.; Kästner, J. *J. Phys. Chem. B* **2017**, *121*, 5347.
(47) Cohen, S.; Kumar, D.; Shaik, S. *J. Am. Chem. Soc.* **2006**, *128*, 2649.
(48) Aldag, C.; Gromov, I. A.; García-Rubio, I.; von Koenig, K.; Schlichting, I.; Jaun, B.; Hilvert, D. *Proc. Natl. Acad. Sci. U. S. A.* **2009**, *106*, 5481.
(49) Jiang, Y.; Sivaramakrishnan, S.; Hayashi, T.; Cohen, S.; Moënne-Loccoz, P.; Shaik, S.; Ortiz de Montellano, P. R. *Angew. Chem., Int. Ed.* **2009**, *48*, 7193.
(50) Lai, W.; Chen, H.; Cho, K.-B.; Shaik, S. *J. Phys. Chem. A* **2009**, *113*, 11763.
(51) Jiang, Y.; Ortiz de Montellano, P. R. *Inorg. Chem.* **2008**, *47*, 3480.
(52) Vandemeulebroucke, A.; Aldag, C.; Stiebritz, M. T.; Reiher, M.; Hilvert, D. *Biochemistry* **2015**, *54*, 6692.
(53) Shaik, S.; Cohen, S.; Wang, Y.; Chen, H.; Kumar, D.; Thiel, W. *Chem. Rev.* **2010**, *110*, 949.
(54) Sivaramakrishnan, S.; Ouellet, H.; Matsumura, H.; Guan, S.; Moënne-Loccoz, P.; Burlingame, A. L.; Ortiz de Montellano, P. R. *J. Am. Chem. Soc.* **2012**, *134*, 6673.
(55) Onderko, E. L.; Silakov, A.; Yosca, T. H.; Green, M. T. *Nat. Chem.* **2017**, *9*, 623.
(56) Cong, Z.; Kinemuchi, H.; Kurahashi, T.; Fujii, H. *Inorg. Chem.* **2014**, *53*, 10632.
(57) Pan, Z.; Horner, J. H.; Newcomb, M. *J. Am. Chem. Soc.* **2008**, *130*, 7776.
(58) Baldwin, J. E.; Bradley, M. *Chem. Rev.* **1990**, *90*, 1079.
(59) Roach, P. L.; Clifton, I. J.; Hensgens, C. M. H.; Shibata, N.; Schofield, C. J.; Hajdu, J.; Baldwin, J. E. *Nature* **1997**, *387*, 827.
(60) Roach, P. L.; Clifton, I. J.; Fülöp, V.; Harlos, K.; Barton, G. J.; Hajdu, J.; Andersson, I.; Schofield, C. J.; Baldwin, J. E. *Nature* **1995**, *375*, 700.
(61) Burzlaff, N. I.; Rutledge, P. J.; Clifton, I. J.; Hensgens, C. M. H.; Pickford, M.; Adlington, R. M.; Roach, P. L.; Baldwin, J. E. *Nature* **1999**, *401*, 721.
(62) Clifton, I. J.; Ge, W.; Adlington, R. M.; Baldwin, J. E.; Rutledge, P. J. *FEBS Lett.* **2013**, *587*, 2705.
(63) Tamanaha, E.; Zhang, B.; Guo, Y.; Chang, W. C.; Barr, E. W.; Xing, G.; St. Clair, J.; Ye, S.; Neese, F.; Bollinger, J. M., Jr.; Krebs, C. *J. Am. Chem. Soc.* **2016**, *138*, 8862.
(64) Brazeau, B. J.; Lipscomb, J. D. *Biochemistry* **2000**, *39*, 13503.
(65) Brazeau, B. J.; Wallar, B. J.; Lipscomb, J. D. *J. Am. Chem. Soc.* **2001**, *123*, 10421.
(66) Xue, G.; De Hont, R.; Münck, E.; Que, L., Jr. *Nat. Chem.* **2010**, *2*, 400.
(67) Truhlar, D. G. *J. Phys. Org. Chem.* **2010**, *23*, 660.
(68) Klinker, E. J.; Shaik, S.; Hirao, H.; Que, L., Jr. *Angew. Chem., Int. Ed.* **2009**, *48*, 1291.
(69) Dutton, P. L.; Munro, A. W.; Scrutton, N. S.; Sutcliffe, M. J. *Philos. Trans. R. Soc., B* **2006**, *361*, 1293.
(70) Williams, I. H. *J. Phys. Org. Chem.* **2010**, *23*, 685.
(71) Armarego, W. L. F.; Chai, C. Purification of Organic Chemicals. *Purification of Laboratory Chemicals*, 7th ed.; Butterworth-Heinemann: Boston, 2013; Chapter 4, pp 103−554.
(72) Halfen, J. A.; Young, V. G., Jr. *Chem. Commun.* **2003**, 2894.
(73) Fiedler, A. T.; Halfen, H. L.; Halfen, J. A.; Brunold, T. C. *J. Am. Chem. Soc.* **2005**, *127*, 1675.
(74) McDonald, A. R.; Bukowski, M. R.; Farquhar, E. R.; Jackson, T. A.; Koehntop, K. D.; Seo, M. S.; De Hont, R. F.; Stubna, A.; Halfen, J. A.; Münck, E.; Nam, W.; Que, L., Jr. *J. Am. Chem. Soc.* **2010**, *132*, 17118.
(75) *Jaguar*, Version 8.0; Schrödinger, LLC: New York, 2011.
(76) Bochevarov, A. D.; Harder, E.; Hughes, T. F.; Greenwood, J. R.; Braden, D. A.; Philipp, D. M.; Rinaldo, D.; Halls, M. D.; Zhang, J.; Friesner, R. A. *Int. J. Quantum Chem.* **2013**, *113*, 2110.
(77) Becke, A. D. *J. Chem. Phys.* **1993**, *98*, 5648.
(78) Becke, A. D. *Phys. Rev. A: At., Mol., Opt. Phys.* **1988**, *38*, 3098.
(79) Lee, C.; Yang, W.; Parr, R. G. *Phys. Rev. B: Condens. Matter Mater. Phys.* **1988**, *37*, 785.
(80) Hariharan, P. C.; Pople, J. A. *Theor. Chim. Acta* **1973**, *28*, 213.
(81) Francl, M. M.; Pietro, W. J.; Hehre, W. J.; Binkley, J. S.; Gordon, M. S.; DeFrees, D. J.; Pople, J. A. *J. Chem. Phys.* **1982**, *77*, 3654.

DOI: 10.1021/jacs.7b11300
J. Am. Chem. Soc. 2017, 139, 18705−18713

(82) Hay, P. J.; Wadt, W. R. *J. Chem. Phys.* **1985**, *82*, 299.
(83) Johansson, A. J.; Blomberg, M. R. A.; Siegbahn, P. E. M. *J. Chem. Phys.* **2008**, *129*, 154301.
(84) Johansson, A. J.; Blomberg, M. R. A.; Siegbahn, P. E. M. *J. Phys. Chem. C* **2007**, *111*, 12397.
(85) Janardanan, D.; Usharani, D.; Chen, H.; Shaik, S. *J. Phys. Chem. Lett.* **2011**, *2*, 2610.
(86) Hratchian, H. P.; Schlegel, H. B. *J. Chem. Phys.* **2004**, *120*, 9918.
(87) Hratchian, H. P.; Schlegel, H. B. In *Theory and Applications of Computational Chemistry*; Frenking, G., Kim, K. S., Scuseria, G. E., Eds.; Elsevier: Amsterdam, 2005; p 195.
(88) Hratchian, H. P.; Schlegel, H. B. *J. Chem. Theory Comput.* **2005**, *1*, 61.
(89) Frisch, M. J.; Trucks, G. W.; Schlegel, H. B.; Scuseria, G. E.; Robb, M. A.; Cheeseman, J. R.; Scalmani, G.; Barone, V.; Mennucci, B.; Petersson, G. A.; Nakatsuji, H.; Caricato, M.; Li, X.; Hratchian, H. P.; Izmaylov, A. F.; Bloino, J.; Zheng, G.; Sonnenberg, J. L.; Hada, M.; Ehara, M.; Toyota, K.; Fukuda, R.; Hasegawa, J.; Ishida, M.; Nakajima, T.; Honda, Y.; Kitao, O.; Nakai, H.; Vreven, T.; Montgomery, J. A., Jr.; Peralta, J. E.; Ogliaro, F.; Bearpark, M. J.; Heyd, J.; Brothers, E. N.; Kudin, K. N.; Staroverov, V. N.; Kobayashi, R.; Normand, J.; Raghavachari, K.; Rendell, A. P.; Burant, J. C.; Iyengar, S. S.; Tomasi, J.; Cossi, M.; Rega, N.; Millam, N. J.; Klene, M.; Knox, J. E.; Cross, J. B.; Bakken, V.; Adamo, C.; Jaramillo, J.; Gomperts, R.; Stratmann, R. E.; Yazyev, O.; Austin, A. J.; Cammi, R.; Pomelli, C.; Ochterski, J. W.; Martin, R. L.; Morokuma, K.; Zakrzewski, V. G.; Voth, G. A.; Salvador, P.; Dannenberg, J. J.; Dapprich, S.; Daniels, A. D.; Farkas, Ö.; Foresman, J. B.; Ortiz, J. V.; Cioslowski, J.; Fox, D. J. *Gaussian 09*; Gaussian, Inc.: Wallingford, CT, 2009.
(90) Duncan, W. T.; Bell, R. L.; Truong, T. N. *J. Comput. Chem.* **1998**, *19*, 1039.
(91) Eckart, C. *Phys. Rev.* **1930**, *35*, 1303.
(92) Eyring, H. *J. Chem. Phys.* **1935**, *3*, 107.
(93) Glendening, D. E.; Reed, A. E.; Carpenter, J. E.; Weinhold, F. *NBO*, version 3.1; University of Wisconsin: Madison, WI, 1992.
(94) Wiberg, K. B. *Tetrahedron* **1968**, *24*, 1083.

NOTE ADDED AFTER ASAP PUBLICATION

Equation 1b was corrected on December 13, 2017.

DOI: 10.1021/jacs.7b11300
J. Am. Chem. Soc. 2017, 139, 18705−18713